Published in final edited form as:
Biomaterials. 2012 January ; 33(1): 137–145. doi:10.1016/j.biomaterials.2011.09.057.

Tissue engineering bone-ligament complexes using fiber-guiding scaffolds

Chan Ho Park[1,2], **Hector F. Rios**[2], **Qiming Jin**[2], **James V. Sugai**[2], **Miguel Padial-Molina**[2], **Andrei D. Taut**[2], **Colleen L. Flanagan**[1], **Scott J. Hollister**[1,4], and **William V. Giannobile**[1,2,3,*]

[1]Department of Biomedical Engineering, University of Michigan College of Engineering, 1101 Beal, Ann Arbor, MI 48109 USA

[2]Department of Periodontics and Oral Medicine, University of Michigan School of Dentistry, 1011 N. University Ave., Ann Arbor, MI 48109 USA

[3]Michigan Center for Oral Health Research, 24 Frank Lloyd Wright Dr., Lobby M, Box 422, Ann Arbor, MI 48106 USA

[4]Department of Surgery, University of Michigan School of Medicine, 1500 East Medical Center Drive, Ann Arbor MI 48109 USA

Abstract

Regeneration of bone-ligament complexes destroyed due to disease or injury is a clinical challenge due to complex topologies and tissue integration required for functional restoration. Attempts to reconstruct soft-hard tissue interfaces have met with limited clinical success. In this investigation, we manufactured biomimetic fiber-guiding scaffolds using solid free-form fabrication methods that custom fit complex anatomical defects to guide functionally-oriented ligamentous fibers *in vivo*. Compared to traditional, amorphous or random-porous polymeric scaffolds, the use of perpendicularly oriented microchannels provides better guidance for cellular processes anchoring ligaments between two distinct mineralized structures. These structures withstood biomechanical loading to restore large osseous defects. Cell transplantation using hybrid scaffolding constructs with guidance channels resulted in predictable oriented fiber architecture, greater control of tissue infiltration, and better organization of ligament interface than random scaffold architectures. These findings demonstrate that fiber-guiding scaffolds drive neogenesis of triphasic bone-ligament integration for a variety of clinical scenarios.

Keywords

Regenerative medicine; regeneration; tissue interfaces; rapid prototyping; biomimetics; wound repair

*Corresponding author. Najjar Endowed Professor of Dentistry & Biomedical Engineering, Departments of Periodontics & Oral Medicine and Department of Biomedical Engineering University of Michigan, Ann Arbor MI 48109-1078, USA. Tel: +1-734-998-1468; Fax: +1-734-998-6900; wgiannob@umich.edu (Giannobile, W.V.).

1. INTRODUCTION

The development and maintenance of a number of complex hard/soft tissue interfaces determine the function and structure of several organs such as the cranial sutures, phalanges, joints, and periodontia. The integrity of these functional interfaces is oftentimes compromised during chronic degenerative diseases, trauma or during acquired and developmental deformities. Loss of functional interfaces adversely affects quality of life. For example, there are greater than 50 million US adults afflicted with severe periodontal disease, the leading cause of tooth loss [1]. Today, the complete regeneration of the structure and function of these important multi-tissue interfaces is unpredictable in the clinical arena [2]. Therefore, the ability to regenerate soft/hard tissue interfaces could have significant clinical impact. The difficulty, however, is that these interfaces represent a complex interplay between multiple cell types, multiple growth factors, and extremely complex matrix topologies. Better understanding of how to integrate synthetic, designed scaffold matrices with multiple cell/growth factor delivery is critical to advancing the engineering of biological interfaces. The goal of this study was to specifically study how one design feature, oriented scaffold channels, affects a tri-phasic tissue interface: cementum-periodontal ligament-bone interface using multiple cell therapy in an *in vivo* model of craniofacial injury.

Of significant interest for craniofacial and appendicular musculoskeletal systems is the ability to engineer bone-ligament interfaces [3–6]. Periodontal engineering is especially challenging, as it requires a triphasic interface between three different tissues: cementum (hard tissue), periodontal ligament (PDL; soft tissue), and bone (hard tissue). The integration of polarized anchoring fibers oriented to a mineralizing surface promotes adequate maturation and important biomechanical properties that regulate tissue adaptability and its long-term stability. Many different approaches have been studied to encourage spatiotemporal control of multi-tissue formation and integration [7, 8] such as reconstruction of soft/hard tissue complexes [6, 9–12], topographical designs to regulate cells [13–17], or microenvironment development for the control of stem cell fates [18, 19]. In addition, reconstructive therapies are increasingly incorporating more precise anatomic scaffold systems such as transplant decellularized/recellularized organs constructs [20–23] or rapid prototyped biomaterials [24–26].

Recently, we have designed an image-based, customized tissue-guiding interfacial scaffold to enhance the formation of mineralized and fibrous connective tissue interfaces. The specialized architecture and characteristic surface topography was shown not only to support the formation of multiple tissues but also facilitate their proper integration when implanted in an ectopic model [27]. By using this scaffold at tooth-ligament complexes in a standardized surgically generated defect model, the regeneration capacity of this system with appropriate biologics can be better evaluated as a precursor to clinical application [1, 28, 29]. A fiber-guiding scaffold system could promote and enhance the formation and integration of the three main structural components of tooth-ligament complexes (bone, ligament and the tooth surface cementum) required for functional stability and biomechanical loading. We hypothesize that a fiber-guiding scaffold with controlled 3D pore architecture will enhance tooth- ligament-bone regeneration within surgically created defects *in vivo*, especially compared to more widely used porogen-leached scaffolds with random 3D pore architecture. We tested this hypothesis by evaluating: 1) If alveolar bone formation could be induced in close proximity to a mineralized surface with an interposed ligament interface between the two mineralized segments; and 2) if the incorporation of micro-channels in the ligamentous portion of the scaffold promoted the polarization of the ligament fibroblasts, enhancing fiber formation and orientation that would lead to optimal

anchoring of ligament structures to the tooth mineralized surface and supportive adjacent alveolar bone.

2. MATERIALS AND METHODS

2.1. Design and fabrication of fiber-guiding scaffold

Based on the designed and developed micro-architecture [27], micro-CT (eXplore Locus SP, GE Healthcare Inc., London, ON Canada) was utilized to generate a medical image-dataset with $18 \times 18 \times 18 \mu m^3$ voxel size after creating a periodontal fenestration defect on the cadaver mandible. This model matched for the *in vivo* experiments was utilized for topographical adaptation of the scaffold surface to the defect. The created STL image data format was imported to Unigraphics NX 5.0 (Siemens PLM software, Plano, TX USA). Three cylindrical-shaped PDL fiber-guiding architectures per layer were designed with 0.225mm diameter and 0.250mm distance from the tooth surface (Fig. 1b. red-colorized). Each of the PDL structure-supporting layers had 0.175mm thick interconnective space between PDL and bone regions (Fig. 1b). The PDL interface architecture was designed to have a 2μl-cell loading capacity. The bone region was designed with 4μl volume to contain cultivated cells. To improve the anatomical scaffold-adaptation to the fenestration defect, Magics 15 (Materialise Inc. Leuven, Belgium) was used to topologically subtract the STL-generated defect from the designed scaffold feature and create 3-D surface topology (Fig. 1b, d–f). After dissolving the Protobuild (Solidscape Inc.) of produced wax molds by 3-D rapid prototyping wax printer (ModelMaker II; Solidscape Inc., Merrimack, NH) in 70% ethanol, 25wt/v poly-ε-caprolactone solution (PCL; MW 43-50kDa) in acetone was casted in fabricated molds. BioAct® VSO (Petroferm Inc. Gurnee, IL) was used to remove the wax materials, Protosupport (Solidscape Inc.) for 2–3d and the remained BioAct® VSO was dissolved in 100% ethanol for 1–2 d (Fig. 1c). All scaffolds were stored at −20°C and sterilized in 70% ethanol 3d before cell seeding.

2.2. Fabrication of random designed scaffold

25wt/v% PCL solution was made in 1,4-dioxane. 250–425μm salt particles were added to PCL in 1,4-dioxane solution with the volume ratio 50:50. Homogeneously dispersed particle suspension was frozen using liquid nitrogen. The solidified PCL in 1,4-dioxane blocks were stored at −80°C for 1 d and dioxane solvent was removed through freeze-drying at −15°C for 4 d. Salt particles were then dissolved in distilled water for 5–7 d and the scaffolds were dried in the vacuum at room temperature for 24–48 h. PCL blocks were cut with approximate dimension $3 \times 2 \times 2\ mm^3$. All scaffolds were stored at −20°C and sterilized in 70% ethanol 3 d before cell seeding.

2.3. Adaptation evaluation of the fiber-guiding scaffold and tooth root topography using micro-CT

PCL fiber-guiding scaffolds were immersed in 35% barium sulphate ($BaSO_4$) in distilled water was used to obtain higher intensity and greyscale Hounsfield Unit (HU) values than mineralized tissues (Supplementary Fig. 1a). The harvested rat mandible was micro-CT scanned with/without the scaffold. On the 2-D coronal section, the 5 mm distance from the border of the dental pulp was selected to cover tooth dentin, PDL interface, and middle of bone region and analyzed using the HU-based histogram. As we developed previously [27], the adaptation ratio was calculated using total length of PDL interface and the linear gap distance between the tooth root surface and PDL architecture (Fig. 1g). Each scaffold in triplicate possessed four different layers and three PDL architectures per layer.

2.4. Surface characterization of scaffolds by scanning electron microscope

The random designed scaffold and the fiber-guiding scaffold were evaluated for surface morphologies using the Environmental Scanning Electron Microscope (ESEM; Philips XL30E SEM FEI Company, Hillsboro, OR USA). The accelerating voltage was 10.0kV.

2.5. Human ligament cell culture and gene transfer

Primary human periodontal ligament cells (hPDL) in passage 4–5 were cultivated from 3 healthy human patients in Dulbecco's Modified Eagle Medium (DMEM; Gibco BRL Life Technologies Inc., Grand Island, NY USA) including 10% fetal bovine serum, antibiotics (100 units/ml penicillin and 100 μg/ml streptomycin) and 2 mm glutamine. The ligament cells were cultured in a humidified atmosphere of 5% CO_2 in air at 37°C and infected with AdCMV-BMP-7, recombinant adenovirus-encoding murine bone morphogenetic protein-7 (BMP-7), at a multiplicity of infection (MOI) of 200 and incubated for 1 d before cell seeding into the random design scaffolds and fiber-guiding scaffolds.

2.6. Cell seeding in random designed scaffold and fiber-guiding scaffold structure

Bovine plasma fibrinogen was dissolved in DMEM to make a 5mg/ml concentration and sterilized with a 0.2μm syringe filter. 2.4×10^5 hPDL cells/scaffold and 2.4×10^5 Ad-BMP-7-hPDL cells/scaffold were suspended within fibrinogen solution for hPDL-seeded and Ad-BMP-7-hPDL-seeded groups in the random-porous scaffolds, respectively. Bovine plasma thrombin was dissolved in Hanks' Balanced Salt Solution at 100 U/ml concentration. The cell-suspended fibrinogen solution was dropped into the scaffolds and those group scaffolds were incubated in 6 h prior to surgery. For the hPDL cell-seeded fiber-guiding scaffold group, the PDL interface and the bone region required 0.4×10^5 hPDL and 0.6×10^5 hPDL, respectively. For the Ad-BMP-7-hPDL-seeded scaffolds, the PDL interface and the bone region needed 0.4×10^5 hPDLs and 0.6×10^5 Ad-BMP-7-hPDLs in fibrinogen solution. During the scaffold implant surgery, thrombin solution was added to the incubated random-porous scaffolds and fiber-guiding scaffolds with the thrombin/fibrinogen volume ratio, 1:5.

2.7. Surgically created periodontal fenestration defect in the in-vivo model system

48 athymic rats (approx. weight 250g acquired from Charles River Laboratories Inc., Wilmington) were used. With 3 and 6 week time-points, 4 different groups were designed: 1) hPDL transplanted random-porous scaffolds, 2) hPDL transplanted fiber-guiding scaffolds, 3) Ad-BMP-7-hPDL seeded random-porous scaffolds, and 4) hPDL (ligament interface) and Ad-BMP-7-hPDL (bone region) transplanted fiber-guiding scaffolds. Ad-BMP-7-hPDL was the adenovirus encoding BMP-7 transduced hPDL cells. General anesthesia was performed with ketamine (90mg/kg) and xylazine (10mg/kg) for the initial periodontal defect creation surgery. Ophthalmic ointment was applied to prevent irritation and relieve eye dryness during surgery. A single periodontal fenestration defect per animal was created on the buccal side of the mandible. The standardized fenestration defect ($3\times2mm^2$ dimension)[45] exposed the distal root surface of the 1st molar tooth (d-M1) (Fig. 1a). The cementum layer on the exposed root surface was removed and recessed to expose the dentin surface. Each cell-seeded scaffold was implanted into the fenestration defect. The muscle and skin incisions were sutured and closed using surgical staples, respectively. Analgesic (5mg/kg; Carprofen), was administrated subcutaneously for 24 h post-surgery. Animals were euthanized using CO_2 for biopsy harvest. All animal surgeries were performed under a protocol approved by the University of Michigan University Committee on Use and Care of Animals.

2.8. Quantitative and qualitative micro-CT analysis

After fixing harvested rat mandibles in 10% buffered formalin phosphate solution for 1 day, micro-CT (GE Healthcare Inc.) scanned them with 18 × 18 × 18μm^3 voxel size. Based on the HU greyscale level, mineralized tissue formation was quantified by MicroView Analysis + 2.1.2 (GE Healthcare Inc.). The regions of interests (ROIs)for the assessment of mineralized tissue formation were created using the following criteria: horizontal region of entire defect and vertically recessed tooth-root surface for tooth-supporting and non tooth-supporting structures (Fig. 2a,b).

2.9. Histomorphometric analysis for fibrous tissue formation and angulation with hematoxylin and eosin (H&E) staining

After the micro-CT scanning, the harvested mandibulae were decalcified in 10% ethylene diaminetetraacetic acid (EDTA) for 4 weeks and embedded in paraffin blocks for histological sectioning and H&E staining. ImageJ (NIH, USA) was used to measure angular orientation of fibrous ligament tissues.

2.10. Immunofluorescence staining to determine functional tissue formation and restoration

Immunofluorescence expression (Fig. 3i–p) and quantitative analysis (Fig. 4e–l and Suppl. Fig. 3) were performed to determine cell morphologies with actin 10 (green), functional ligament tissues with periostin (red), and cell nuclei with 4',6-diamidino-2-phenylindole (DAPI; blue). F-actin distribution was revealed with Alexa Fluor® 488 phalloidin (5:200 dilution; Invitrogen Corporation). Fluorescence staining to periostin was performed on paraffin sections using an affinity purified rabbit polyclonal antibody (1:200 dilution; ab14041, Abcam, Inc., Cambridge, MA USA). Immunological reaction was visualized by using a sheep polyclonal secondary antibody to rabbit conjugated to Texas Red (TR) (1:200 dilution; ab6793-1, Abcam). The sections were then treated with an antifade agent containing DAPI and covered with glass coverslips. The stained slides were imaged using an OLYMPUS Fluroview 500 confocal microscope.

2.11. Statistical analysis

All data were presented with means ± standard deviation (s.d.). For the scaffold adaptation analysis, one-way ANOVA test with the Bonferroni correction was utilized. The comparisons of bone parameters from micro-CT and the ligament angulation calculation were performed using two-tailed independent-samples *t* test. For the tooth-supporting and non tooth-supporting tissue formations, the two-sample paired t-test was utilized.

3. RESULTS

3.1. Geometric Fit of Designed Scaffold to Periodontal Osseous Defects

The interface fit between the 3D designed scaffolds and the complex periodontal defect was evaluated by a previously developed adaptation ratio, using microcomputed tomography (micro-CT) generated histograms (Fig. 1a–f) that were segmented at four different levels in an apico-coronal direction (3-D color image in Fig. 1g). From these images, gap distance (d^{gap}) was measured across the ligament space and root surfaces. The adaptation ratio was calculated from d^{gap} and the entire length of ligament interface ($d^{ligament}$; Fig. 1f), with values close to 1 indicating better fit of the scaffold to the defect. The results clearly demonstrated that all the ligament scaffold components (n = 36), conformed extremely well to the defect surface topography (mean ± s.d. = 0.962 ± 0.049; Fig. 1g) (Supplementary Fig. 1b). The porogen-leached scaffolds had a random, tortuous 3D porous architecture (Fig. 1h), while the fiber-guiding scaffolds displayed an external architecture customized to fit the

anatomic defect and a micro-groove patterned surface topography with a characteristic micro-porosity as seen by scanning electron microscopic SEM (Fig. 1i).

3.2. Quantification of mineralized tissue formation in periodontal defects using micro-computed tomography (micro-CT)

In sectional views of micro-CT images, different spatial growth patterns of mineralized tissues were qualitatively identified (Fig. 2a–c). The random-porous scaffolds with BMP-7 transduced ligament cell transplantation presented larger amounts of mineralized tissue formation with higher density in the outer area of the defect and non tooth-supporting regions (Fig. 2b), whereas the fiber-guiding scaffolds had consistently greater amounts of supporting mineralized tissue formation around the tooth structure (Fig. 2c).

For the quantitative analysis of tooth-supporting tissue formation, a region of interest (ROI) was created [yellow triangles (transverse view) and white dashed-lines (coronal view) within the osseous defects (Fig. 2a–c)]. Bone volume fraction (BVF) and tissue mineral density (TMD) 3 and 6 weeks post-surgery were used to confirm regeneration of tooth-supporting structures (Fig. 2). All fiber-guiding and the untreated ligament cell-seeded random-porous scaffold groups had significantly increased tooth-supporting tissue formation (yellow columns in Supp. Fig. 2c, d) compared to non tooth-supporting structures (red columns in Supp. Fig. 2c, d) at each time point. Contrastingly, the BMP-7 transduced ligament cell-seeded random-porous scaffolds displayed no significant difference between tooth-supporting and non tooth-supporting tissue formation at 3 weeks ($p^{\text{BVF-3week}} > 0.10$; $p^{\text{TMD-3week}} > 0.10$) and there was less tissue-infiltration into the defect and less tooth-supporting mineralized tissue formation at 6 weeks ($p^{\text{BVF-6week}} = 0.03$; $p^{\text{TMD-6week}} = 0.02$; Supp. Fig. 2c, d). In terms of tissue infiltration using gene-mediated delivery, random-porous scaffolds with over 90% porosity displayed limited mineralized tissue in-growth, whereas fiber-guiding scaffolds possessing the geometrical design induced greater amounts and more spatially-directed bone growth. Regarding tooth-supporting alveolar bone neogenesis, the fiber-guiding scaffolds promoted greater mineralized tissue regeneration at both time-points (Fig. 2d–g; $p<0.005$). Overall, none of the experimental groups demonstrated statistically significant differences in the *total* amount of mineralized tissue formation at 6 weeks as assessed on micro-CT digitized serial sections[28] (Supplementary Fig. 2a, b).

3.3. Histomorphometry and Immunofluorescence analyses of functional ligament tissue formation

Using hematoxylin and eosin (H&E) staining, the ligament tissue organization was determined within the bone-ligament complex (Fig. 3a–h). In addition, to evaluate the formation of a mature specialized fibrous connective tissue at the tooth-defect interface, a functional PDL marker molecule known as periostin was targeted for immunofluoresence detection (Fig. 3i–p).

The topographical discrepancies between the two distinct geometric scaffolds (Fig. 1h, i) led to different morphological patterns of tissue healing (Fig. 3). Specifically, the scaffold internal architecture strongly dictated the healing phenotypes at the ligament interface (Fig. 3a–h). Compartmentalized multi–tissue neogenesis was generated with clearly defined ligament directionality (black dash lines in Fig. 3c, d, g, h) in the fiber guiding scaffold design. In contrast, the random design yielded erratically organized tissue healing following the arbitrary random pore orientation of the porogen-leached scaffolds (Fig. 3a, b, e, f). Moreover, cementum-like tissue layers were deposited on the dentin surfaces with fiber-guiding scaffolds (white arrows indicated in Fig. 3a–h) while the ligament cell-seeded randomly oriented geometric approach displayed significantly less mineral layer formation.

Periostin distribution was evaluated by immunofluorescence in the healing areas at 3 and 6 weeks as a marker for PDL tissue maturity, integrity and functionality, indirectly allowing us to evaluate the re-establishment of periodontal function [30] (Fig. 3i–p). Interestingly, the regenerated and oriented ligament tissues displayed dramatically greater periostin immunoreactivity (Fig. 3k, l, o p) compared with the random-porous scaffolds (Fig. 3i, j, m, n and Suppl. Fig. 3). Consequently, it appears that the fiber-guiding system is more likely than the to produce the biomechanically functional environments necessary for the long-term maintenance of periodontal tissue integrity.

3.4. Ligament tissue orientation and stability of interfacial ligament

To quantitatively assess fiber formation and orientation with different groups, the angulation of fiber bundles against the tooth-root surfaces (Fig. 4a–d) was measured. The angulation of regenerated ligament directionality was measured against the dentin surface (Fig. 4d). Compared to the native mature ligament as a reference (mean ± s.d. = 47.3 ± 12.0°; Fig. 4a, d), the random-porous scaffold groups demonstrated less angulation (3 weeks: $p^{\text{ligament}} < 0.0001$; $p^{\text{BMP-7-transduced ligament}} < 0.0001$, 6 weeks: $p^{\text{ligament}} < 0.0001$; $p^{\text{BMP-7-transduced ligament}} < 0.0001$), whereas the fiber-guiding scaffolds displayed no statistically difference in angulation than native ligament tissue (3 weeks: $p^{\text{ligament}} = 0.58$, 6 weeks: $p^{\text{BMP-7-transduced ligament}} = 0.97$) where ligament tissues were oriented with larger angles (at 3 weeks: $p^{\text{BMP-7-transduced ligament}} = 0.002$, 6 weeks: $p^{\text{ligament}} = 0.025$) at both time points compared to random scaffolds (Fig. 4a–c). These results demonstrate that the computer-designed, fiber-guiding scaffolds can guide ligament orientation that is similar to the mature ligaments. In addition to the angle distribution, the lower frequency represented significantly less fibrous tissue formation and organization in the random design groups compared to the fiber-guiding groups (Fig. 4b, c). Therefore, the fiber-guiding scaffolds appear to guide ligament cells with a polarized oblique orientation to the mineralized root surfaces in a more predictable fashion and more similar to native ligament tissue than with traditional, random oriented scaffold design.

The presence of periostin expression furthermore demonstrates stability and maturation of the periodontal ligament matrix [30]. Identification of mature fiber generation from bone to cementum infers increased tissue functionality in regenerated ligament-bone complexes. Moreover, the results suggest a good correlation between designed scaffold topography and functional restoration of regenerated ligamentous tissues. For the semi-quantification of the functionalized ligament interface, the expression level of periostin at the defect sites was analyzed using a color scale based on periostin intensity level (Fig. 4e–l). In 3-D fluorescence intensity profiles, regenerating ligament interfaces in the fiber-guiding groups had higher expression values of periostin than random-porous scaffolds at 3 and 6 weeks (Fig. 4e–l). Moreover, the fiber-guiding scaffold had statistically similar levels to the native ligament interface (Fig. 4g, h, k, l). These groups can represent the early stage of functional restoration in regenerated ligament-bone complexes. Thus, the fiber-guiding scaffold system appears to promote the rearrangement of ligament tissues with fibrous directionalities and rapid establishment of a mature matrix similar to the native ligament.

4. DISCUSSION

Various tissue engineering approaches for reconstitution of multiple tissues have been developed and interfacial tissue engineering has recently emerged as a field of significant interest. Although some progress has been reported on non-directional fibrous tissue neogenesis on bone substrates, the regeneration of ligament-bone two-phase complexes remains a significant challenge, let alone the regeneration of the three-phase dentin-PDL-bone complex [10, 31]. For the functional recovery of the ligament-bone constructs, fibrous connective tissues require orientation against bone surfaces to allow optimal biomechanical

integration. In this *in vivo* study, we have demonstrated an approach for ligament-bone complex interfacial regeneration; namely the use of oriented controlled 3D pores with tissue compartments that match the shape of complex anatomic defects with separate seeding of cells by phenotype. This interfacial scaffold/cell compartment approach enhanced regeneration of functional ligament within a surgically created osseous defect model.

For multi-tissue morphogenesis, It is necessary to seed multiple cell types in 3D space and guide their interaction and communication with controlled architectures, including orientation [32]. Moreover, diverse 3-D physiological conditions can lead to more complicated and unpredictable cell movements [32–34] when compared with the 2-D or *in vitro* culture systems. Although the guidance of 3-D geometric architectures has currently focused on the significant influence over the collective cell responses like migration [33–35] for tissue reorganization and structuralization, there are still limitations to predict or control the directionality of the cell collectiveness *in vivo* under 3-D physiological conditions for tissue formation or wound healing [32]. To coordinate multiple tissue complex regeneration and configuration in a single system, controlling collective cell and tissue compartmentalization are required. Therefore, one key factor such as the scaffold topography or architectural design enhances the morphogenesis, organization, and functionalization of multiple tissue interfaces [32].

In 3-D conditions, compartmentalized multi-tissue formation and fibrous connective tissue orientation were promoted with cell migration following the designed topography. The angular orientation of ligament tissues against the dentin surface was histomorphometrically observed with calcified tissue layer deposition (Fig. 3). Moreover, immunohistochemical periostin expression demonstrated PDL integrity and as a marker for interfacial matrix maturation and stability (Fig. 4). Because the system can provide the 3-D fiber-guidable topographies, fibrous connective tissues angulation and directionality was statistically the same as native ligament interface. More remarkably, by maintaining a continuous, biomechanical-sensitive environment, the functionality of regenerated ligament-bone complexes around the osseous defect can be restored predictably and sustained over time. The tooth model system used here allows for multi-tissue evaluation of two different mineralized structures with an intervening ligamentous structure required for biomechanical loading and function. The advantage of this model system is that various biomechanical stimulations can be transmitted directly to experimental defects while the osseous defect model can also prevent physical damage of scaffolds at the implantation sites. Hence, this periodontal osseous defect model represents a valuable tool to explore and explain the interaction between physical topographies and tissue morphogenesis using a standardized 3-D physiological environment with consistent biomechanical stimulation. Periostin, a mechanically regulated matricellular molecule was utilized to investigate the integrity of the regenerated periodontal ligament interfaces [30, 36, 37]. Periostin is also an important molecule in extracellular-matrix mediated tissue healing and homeostasis in a number of organs such as the heart, periodontium and bone [30, 38–42]. Periostin modulates the biomechanical properties of specialized fibrous connective tissues by influencing collagen fibrilogenesis [43]. The identification of periostin in the newly formed interfacial tissue was therefore utilized to infer the degree of tissue maturation and stability of the periodontal fibers. Therefore, via periostin, we could track the maturation and re-functionalization of regenerated interfacial ligaments and quantify the periostin expression levels at native and regenerated regions (Fig. 4e–l).

The biomimetic architecture achieved here provides a promising platform for craniofacial and musculoskeletal multiple tissue interface reconstruction. Moreover, the micro-architecture can induce the functional integrity of regenerated ligament-bone complexes. Although we just focused on the periodontal complex regeneration here, the anatomical

design with the fiber-guiding internal geometries can be applied to diverse clinical applications. In conclusion, this study clearly demonstrates that designed 3D scaffolds with controlled, oriented fiber channels were essential to create functional ligamentous interfaces with appropriate cell and fiber orientation between bone and dentin tissue in an *in vivo* periodontal defect model. Furthermore, the ability to compartmentalize different cell phenotypes in physical space was important to create the distinct tissue regions.

5. CONCLUSIONS

This in vivo study demonstrates that fiber-guiding hybrid scaffolds promote triphasic tissue regeneration with the compartmentalization of hard and soft tissue structures. The regenerated complex drives functional restoration of periodontal tissues under biomechanical loading conditions.

Supplementary Material

Refer to Web version on PubMed Central for supplementary material.

Acknowledgments

The study was supported by NIH/NIDCR DE 13397.

References

1. Pihlstrom BL, Michalowicz BS, Johnson NW. Periodontal diseases. Lancet. 2005; 366(9499):1809–1820. [PubMed: 16298220]
2. Hughes FJ, Ghuman M, Talal A. Periodontal regeneration: a challenge for the tissue engineer? Proc Inst Mech Eng H. 2010; 224(12):1345–1358. [PubMed: 21287824]
3. Guldberg RE. Spatiotemporal delivery strategies for promoting musculoskeletal tissue regeneration. J Bone Miner Res. 2009; 24(9):1507–1511. [PubMed: 19653806]
4. Mao JJ, Giannobile WV, Helms JA, Hollister SJ, Krebsbach PH, Longaker MT, et al. Craniofacial tissue engineering by stem cells. J Dent Res. 2006; 85(11):966–979. [PubMed: 17062735]
5. Place ES, Evans ND, Stevens MM. Complexity in biomaterials for tissue engineering. Nat Mater. 2009; 8(6):457–470. [PubMed: 19458646]
6. Spalazzi JP, Dagher E, Doty SB, Guo XE, Rodeo SA, Lu HH. In vivo evaluation of a multiphased scaffold designed for orthopaedic interface tissue engineering and soft tissue-to-bone integration. J Biomed Mater Res A. 2008; 86(1):1–12. [PubMed: 18442111]
7. Yang PJ, Temenoff JS. Engineering orthopedic tissue interfaces. Tissue Eng Part B Rev. 2009; 15(2):127–141. [PubMed: 19231983]
8. Wang DA, Varghese S, Sharma B, Strehin I, Fermanian S, Gorham J, et al. Multifunctional chondroitin sulphate for cartilage tissue-biomaterial integration. Nat Mater. 2007; 6(5):385–392. [PubMed: 17435762]
9. Phillips JE, Burns KL, Le Doux JM, Guldberg RE, Garcia AJ. Engineering graded tissue interfaces. Proc Natl Acad Sci U S A. 2008; 105(34):12170–12175. [PubMed: 18719120]
10. Moffat KL, Sun WH, Pena PE, Chahine NO, Doty SB, Ateshian GA, et al. Characterization of the structure-function relationship at the ligament-to-bone interface. Proc Natl Acad Sci U S A. 2008; 105(23):7947–7952. [PubMed: 18541916]
11. Schek RM, Taboas JM, Segvich SJ, Hollister SJ, Krebsbach PH. Engineered osteochondral grafts using biphasic composite solid free-form fabricated scaffolds. Tissue Eng. 2004; 10(9–10):1376–1385. [PubMed: 15588398]
12. Hong L, Mao JJ. Tissue-engineered rabbit cranial suture from autologous fibroblasts and BMP2. J Dent Res. 2004; 83(10):751–756. [PubMed: 15381713]
13. Ding Y, Sun J, Ro HW, Wang Z, Zhou J, Lin NJ, et al. Thermodynamic Underpinnings of Cell Alignment on Controlled Topographies. Adv Mater. 2011; 23(3):421–425. [PubMed: 20717992]

14. Petrie RJ, Doyle AD, Yamada KM. Random versus directionally persistent cell migration. Nat Rev Mol Cell Biol. 2009; 10(8):538–549. [PubMed: 19603038]
15. Doyle AD, Wang FW, Matsumoto K, Yamada KM. One-dimensional topography underlies three-dimensional fibrillar cell migration. J Cell Biol. 2009; 184(4):481–490. [PubMed: 19221195]
16. Geiger B, Spatz JP, Bershadsky AD. Environmental sensing through focal adhesions. Nat Rev Mol Cell Biol. 2009; 10(1):21–33. [PubMed: 19197329]
17. Kim DH, Wong PK, Park J, Levchenko A, Sun Y. Microengineered platforms for cell mechanobiology. Annu Rev Biomed Eng. 2009; 11:203–233. [PubMed: 19400708]
18. Engler AJ, Sen S, Sweeney HL, Discher DE. Matrix elasticity directs stem cell lineage specification. Cell. 2006; 126(4):677–689. [PubMed: 16923388]
19. Discher DE, Janmey P, Wang YL. Tissue cells feel and respond to the stiffness of their substrate. Science. 2005; 310(5751):1139–1143. [PubMed: 16293750]
20. Ott HC, Clippinger B, Conrad C, Schuetz C, Pomerantseva I, Ikonomou L, et al. Regeneration and orthotopic transplantation of a bioartificial lung. Nat Med. 2010; 16(8):927–933. [PubMed: 20628374]
21. Uygun BE, Soto-Gutierrez A, Yagi H, Izamis ML, Guzzardi MA, Shulman C, et al. Organ reengineering through development of a transplantable recellularized liver graft using decellularized liver matrix. Nat Med. 2010; 16(7):814–820. [PubMed: 20543851]
22. Atala A. Engineering organs. Curr Opin Biotechnol. 2009; 20(5):575–592. [PubMed: 19896823]
23. Ott HC, Matthiesen TS, Goh SK, Black LD, Kren SM, Netoff TI, et al. Perfusion-decellularized matrix: using nature's platform to engineer a bioartificial heart. Nat Med. 2008; 14(2):213–221. [PubMed: 18193059]
24. Lee CH, Cook JL, Mendelson A, Moioli EK, Yao H, Mao JJ. Regeneration of the articular surface of the rabbit synovial joint by cell homing: a proof of concept study. Lancet. 2010; 376(9739): 440–448. [PubMed: 20692530]
25. Grayson WL, Frohlich M, Yeager K, Bhumiratana S, Chan ME, Cannizzaro C, et al. Engineering anatomically shaped human bone grafts. Proc Natl Acad Sci U S A. 2010; 107(8):3299–3304. [PubMed: 19820164]
26. Hollister SJ. Porous scaffold design for tissue engineering. Nat Mater. 2005; 4(7):518–524. [PubMed: 16003400]
27. Park CH, Rios HF, Jin Q, Bland ME, Flanagan CL, Hollister SJ, et al. Biomimetic hybrid scaffolds for engineering human tooth-ligament interfaces. Biomaterials. 2010; 31(23):5945–5952. [PubMed: 20471083]
28. Chen FM, Zhang J, Zhang M, An Y, Chen F, Wu ZF. A review on endogenous regenerative technology in periodontal regenerative medicine. Biomaterials. 2010; 31(31):7892–7927. [PubMed: 20684986]
29. Darveau RP. Periodontitis: a polymicrobial disruption of host homeostasis. Nat Rev Microbiol. 2010; 8(7):481–490. [PubMed: 20514045]
30. Rios HF, Ma D, Xie Y, Giannobile WV, Bonewald LF, Conway SJ, et al. Periostin is essential for the integrity and function of the periodontal ligament during occlusal loading in mice. J Periodontol. 2008; 79(8):1480–1490. [PubMed: 18672999]
31. Moffat KL, Kwei AS, Spalazzi JP, Doty SB, Levine WN, Lu HH. Novel nanofiber-based scaffold for rotator cuff repair and augmentation. Tissue Eng Part A. 2009; 15(1):115–126. [PubMed: 18788982]
32. Rorth P. Collective cell migration. Annu Rev Cell Dev Biol. 2009; 25:407–429. [PubMed: 19575657]
33. Griffith LG, Swartz MA. Capturing complex 3D tissue physiology in vitro. Nat Rev Mol Cell Biol. 2006; 7(3):211–224. [PubMed: 16496023]
34. Even-Ram S, Yamada KM. Cell migration in 3D matrix. Curr Opin Cell Biol. 2005; 17(5):524–532. [PubMed: 16112853]
35. Cukierman E, Pankov R, Stevens DR, Yamada KM. Taking cell-matrix adhesions to the third dimension. Science. 2001; 294(5547):1708–1712. [PubMed: 11721053]

36. Afanador E, Yokozeki M, Oba Y, Kitase Y, Takahashi T, Kudo A, et al. Messenger RNA expression of periostin and Twist transiently decrease by occlusal hypofunction in mouse periodontal ligament. Arch Oral Biol. 2005; 50(12):1023–1031. [PubMed: 15922993]

37. Wilde J, Yokozeki M, Terai K, Kudo A, Moriyama K. The divergent expression of periostin mRNA in the periodontal ligament during experimental tooth movement. Cell Tissue Res. 2003; 312(3):345–351. [PubMed: 12761672]

38. Shimazaki M, Kudo A. Periostin, acting in regeneration of periodontal ligament, contributes to cardiac healing and tumor capsule formation. Fukuoka Igaku Zasshi. 2009; 100(3):67–74. [PubMed: 19507537]

39. Nakazawa T, Nakajima A, Seki N, Okawa A, Kato M, Moriya H, et al. Gene expression of periostin in the early stage of fracture healing detected by cDNA microarray analysis. J Orthop Res. 2004; 22(3):520–525. [PubMed: 15099630]

40. Nakamura S, Terashima T, Yoshida T, Iseki S, Takano Y, Ishikawa I, et al. Identification of genes preferentially expressed in periodontal ligament: specific expression of a novel secreted protein, FDC-SP. Biochem Biophys Res Commun. 2005; 338(2):1197–1203. [PubMed: 16259954]

41. Kuhn B, del Monte F, Hajjar RJ, Chang YS, Lebeche D, Arab S, et al. Periostin induces proliferation of differentiated cardiomyocytes and promotes cardiac repair. Nat Med. 2007; 13(8): 962–969. [PubMed: 17632525]

42. Dorn GW 2nd. Periostin and myocardial repair, regeneration, and recovery. N Engl J Med. 2007; 357(15):1552–1554. [PubMed: 17928607]

43. Norris RA, Damon B, Mironov V, Kasyanov V, Ramamurthi A, Moreno-Rodriguez R, et al. Periostin regulates collagen fibrillogenesis and the biomechanical properties of connective tissues. J Cell Biochem. 2007; 101(3):695–711. [PubMed: 17226767]

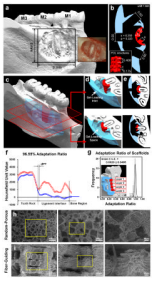

Figure 1.

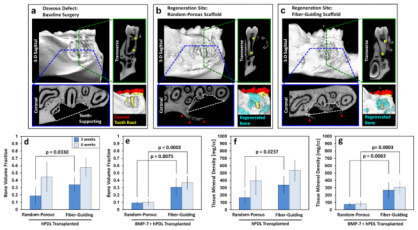

Figure 2.

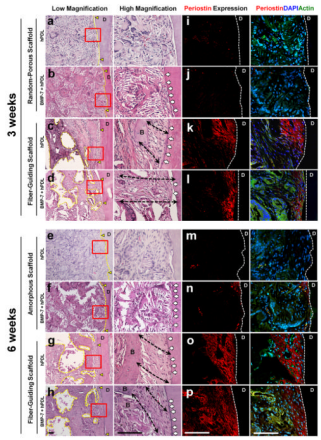

Figure 3.

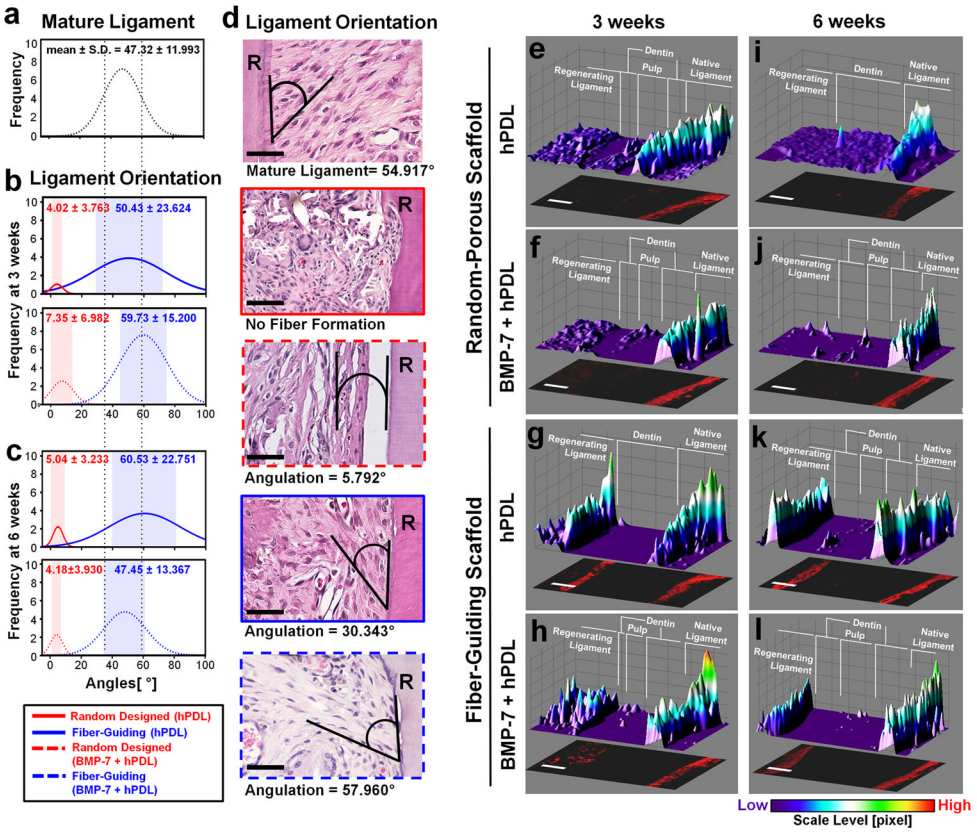

Figure 4.